Published in final edited form as:
Ultrasonics. 2013 March ; 53(3): 727–738. doi:10.1016/j.ultras.2012.10.017.

High-resolution vascular tissue characterization in mice using 55 MHz ultrasound hybrid imaging

Ahmed M. Mahmoud[a,b,*], **Cesar Sandoval**[c], **Bunyen Teng**[d], **Jurgen B. Schnermann**[e], **Karen H. Martin**[d], **S. Jamal Mustafa**[d], and **Osama M. Mukdadi**[c,d]

[a]Center for Ultrasound Molecular Imaging and Therapeutics, Heart and Vascular Institute, University of Pittsburgh and University of Pittsburgh Medical Center, Pittsburgh, PA 15261, United States

[b]Department of Biomedical Engineering, Cairo University, Giza 12613, Egypt

[c]Department of Mechanical and Aerospace Engineering, West Virginia University, Morgantown, WV 26506, United States

[d]Center for Cardiovascular & Respiratory Sciences, West Virginia University, Morgantown, WV 26506, United States

[e]National Institute of Diabetes and Digestive and Kidney Diseases, National Institute of Health, Bethesda, MD 20892, United States

Abstract

Ultrasound and Duplex ultrasonography in particular are routinely used to diagnose cardiovascular disease (CVD), which is the leading cause of morbidity and mortality worldwide. However, these techniques may not be able to characterize vascular tissue compositional changes due to CVD. This work describes an ultrasound-based hybrid imaging technique that can be used for vascular tissue characterization and the diagnosis of atherosclerosis. Ultrasound radiofrequency (RF) data were acquired and processed in time, frequency, and wavelet domains to extract six parameters including time integrated backscatter (T_{IB}), time variance (T_{var}), time entropy (T_E), frequency integrated backscatter (F_{IB}), wavelet root mean square value (W_{rms}), and wavelet integrated backscatter (W_{IB}). Each parameter was used to reconstruct an image co-registered to morphological B-scan. The combined set of hybrid images were used to characterize vascular tissue *in vitro* and *in vivo* using three mouse models including control (C57BL/6), and atherosclerotic apolipoprotein E-knockout (APOE-KO) and APOE/A_1 adenosine receptor double knockout (DKO) mice. The technique was tested using high-frequency ultrasound including single-element (center frequency = 55 MHz) and commercial array (center frequency = 40 MHz) systems providing superior spatial resolutions of 24 μm and 40 μm, respectively. Atherosclerotic vascular lesions in the APOE-KO mouse exhibited the highest values (contrast) of −10.11 ± 1.92 dB, −12.13 ± 2.13 dB, −7.54 ± 1.45 dB, −5.10 ± 1.06 dB, −5.25 ± 0.94 dB, and −10.23 ± 2.12 dB in T_{IB}, T_{var}, T_E, F_{IB}, W_{rms}, W_{IB} hybrid images ($n = 10$, $p < 0.05$), respectively. Control segments of normal vascular tissue showed the lowest values of −20.20 ± 2.71 dB, −22.54 ± 4.54 dB, −14.94 ± 2.05 dB, −9.64 ± 1.34 dB, −10.20 ± 1.27 dB, and −19.36 ± 3.24 dB in same hybrid images ($n = 6$, $p < 0.05$). Results from both histology and optical images showed good agreement with ultrasound findings within a maximum error of 3.6% in lesion estimation. This study demonstrated the feasibility of a high-resolution hybrid imaging technique to diagnose atherosclerosis and characterize plaque components in mouse. In the future, it can be easily

*Corresponding author at: Heart and Vascular Institute, University of Pittsburgh School of Medicine, Pittsburgh, PA 15261, United States. Tel.: +1 412 648 9569; fax: +1 412 624 2264. Mahmouda@upmc.edu (A.M. Mahmoud)..

implemented on commercial ultrasound systems and eventually translated into clinics as a screening tool for atherosclerosis and the assessment of vulnerable plaques.

Keywords

High resolution ultrasound; Tissue characterization; Atherosclerosis; Signal and image processing

1. Introduction

Atherosclerosis is considered one of the main causes of cardiovascular disease (CVD) that is the number one killer globally and the incidence of disease is increasing [1]. According to the American Heart Association Statistics Committee and Stroke Statistics Subcommittee, 1 in 3 people are estimated to have one or more types of CVDs [2]. Genetically modified mouse models provide a powerful tool for understanding the pathogenesis of human cardiovascular diseases like human atherosclerosis [3]. Among available models, the apolipoprotein E-knockout mouse (APOE-KO) that is particularly popular because of its tendency to develop atherosclerotic lesions of similar complexity as those found in humans [4]. In a previous report, our research group has demonstrated that by removing A_1 adenosine receptor (AR) gene from APOE-KO, the resulting development of atherosclerosis in APOE and A_1 AR double knockout mice (DKO) was significantly decreased [5]. Accordingly, availability of these mouse models in cardiovascular research has motivated the development of diagnostic imaging techniques to assess the cardiovascular function.

Several noninvasive imaging techniques have been used for the *in vivo* assessment of CVD including electron-beam computed tomography [6], magnetic resonance imaging [7], positron emission tomography [8], and optical coherent tomography [9]. Although commercial ultrasound scanners have been used to image human hearts, they might not be appropriate in small animal due to their limited spatial resolution (0.3–1 mm). Mice have extremely small arteries (~0.07–1 mm in diameter) and elevated heart rates (500–800 beats/min) which presents a great challenge for commercial ultrasound scanners. High-frequency (>20 MHz) ultrasound systems were developed in order to achieve a spatial resolution of 50 μm or smaller and can provide adequate imaging of mouse vasculature [10].

High-frequency (high-resolution) ultrasound systems have been developed during recent decades. In 1987, Sherar et al. [11] was the first to show the enormous potential of high-frequency ultrasound for tissue imaging. Further developments in high-frequency ultrasound were performed by Sun et al. [12,13] to image small animal hearts providing high-resolution (≤50 μm). Most ultrasound studies on small animals are currently carried out using either custom high-frequency ultrasound systems or the Vevo commercial systems (Vevo 770 and Vevo 2100, VisualSonics Inc., Toronto, ON, Canada). However, the diagnosis, monitoring, or treatment of atherosclerosis may require an imaging system able to provide both quantitative morphological measurements and compositional characterization of the disease. Such quantitative tissue characterization techniques are not available in the aforementioned systems without the use of contrast agents.

Quantitative ultrasonic tissue characterization for the heart has been demonstrated by Miller's group in 1980's [14,15]. They described the potential of using integrated backscatter (IB) measurements to assess dog cardiac tissues using 3.5–5 MHz ultrasound transducers [14]. Bridal et al. reported the use of ultrasonic parameters such as IB and attenuation to characterize plaques in human arteries using high-frequency ultrasound (30–50 MHz), in an *in vitro* study [16]. Tissue characterization techniques were also used to diagnose and identify the composition of atherosclerosis in human arteries using 30 MHz and 40 MHz

intravascular ultrasound imaging (IVUS) [17–19]. These techniques extract parameters from ultrasound backscatters to render virtual histology maps for quantitative assessment of atherosclerosis. IVUS elastography maps were also introduced to characterize atherosclerotic plaque components by measuring mechanical stiffness [20,21]. However, most of the aforementioned techniques are invasive and would not be ideal for monitoring disease longitudinally. Noninvasive cardiovascular ultrasound elastography was recently adopted to characterize atherosclerosis in human carotid artery. However, the resolution of the technique (≥125 μm) is still a limiting factor in small animal models of atherosclerosis [20]. For *in vivo* small animal studies, however, high-resolution (≤50 μm) tissue imaging and characterization shall be required to assess the cardiovascular system and diagnose CVD.

In this study, we demonstrated the feasibility of an ultrasound-based noninvasive tissue characterization algorithm using high resolution (≤40 μm) hybrid imaging, which was applied to diagnose atherosclerotic plaques. The algorithm was applied to RF data collected from both a single-element transducer [22] and a commercial array systems (Vevo 2100) to characterize atherosclerosis in mice. In addition, we investigate the use of novel ultrasonic quantitative parameters extracted from the time and wavelet domains (time variance (T_{var}), time entropy (T_E), wavelet root mean square value (W_{rms}), and wavelet integrated backscatter (W_{IB})) to characterize atherosclerotic plaques and compare with existing parameters (time integrated backscatter (T_{IB}), frequency integrated backscatter (F_{IB})). The technique was tested *in vitro* and *in vivo* using control and atherosclerotic mouse models. This paper is organized as follows. Section 2 describes the ultrasound systems, tissue characterization algorithm, and *in vitro* and *in vivo* experiments. The results are shown and discussed in Sections 3 and 4, respectively. Finally, Section 5 provides the concluding remarks of this study.

2. Materials and methods

2.1. Custom ultrasound system

The high-frequency ultrasound imaging system used for *in vitro* testing was described in [22]. An ultrasound transducer (29–81 MHz) of 55 MHz center frequency and 9.7 mm focal length was used (Olympus NDT Inc., Waltham, MA, USA). Received RF signals were pre-amplified and filtered, then fed to a high-speed (400 MHz) 14-bits waveform digitizer (Signatec Inc., Newport Beach, CA, USA). The imaging system used a PC for control, synchronization, and further signal processing. The PC controlled precisely a two-axis positioning system using ±1 μm resolution (Danaher Corp., Washington, DC, USA). The positioning system was synchronized with the data acquisition to collect ultrasound RF signals continuously *on-the-fly* during the transducer movement down to 8.5 μm apart. A custom user-friendly computer graphical user interface (GUI) was designed using Microsoft Visual C++ (Microsoft Corp., Redmond, WA) for control and data acquisition. Data was then transferred to MATLAB 7.1 (MathWorks, Inc., Natick, MA, USA) for post-processing and image reconstruction. To obtain a high-resolution B-mode ultrasound images, several signal and image processing algorithms were applied to the high-frequency echo signals [22,23]. This ultrasound system provided access to ultrasound data at all processing stages including synthetic aperture focusing (SAF), envelop detection, and final B-mode processed images, which was essential for the tissue characterization technique described below. The SAF procedure was applied using the weighted synthetic aperture focusing to overcome the limited depth of field for a highly focused single-element [24,25]. The system spatial resolution was experimentally evaluated using a B-mode image for an 8 μm tungsten wire immersed in water. The experimental values of the axial and lateral resolutions were approximately measured to be 24 μm and 123 lm, respectively. An average signal to noise

ratio (SNR) of 109 dB was estimated experimentally for the system using a planar reflector (glass plate).

2.2. Quantitative ultrasound tissue characterization

Fig. 1 described the main procedures of the tissue characterization technique. First, a region of interest (ROI) was segmented and extracted from the raw ultrasound data after SAF. ROI was then divided into 2D kernels of small size, such as 0.15 mm × 0.15 mm with approximately 90% overlapping. To reconstruct hybrid images, a vector $S_{i,j}$ was generated for each spatial location (i, j) within the ultrasound scan. This vector was reconstructed from the neighborhood pixels $P_{i,j}$ within the kernel $K_{i,j}$, and defined as:

$$S_{i,j}=\left[\left(P_i-\frac{n}{2},j-\frac{m}{2}\right)\ldots\left(P_{i,j}\right)\ldots\left(P_i+\frac{n}{2},j+\frac{m}{2}\right)\right], \quad (1)$$

where $n+1$ and $m+1$ are the kernel length and width in pixels, respectively. For each spatial location within the ROI, $S_{i,j}$ vector was reconstructed from ultrasound data. This vector was considered a 1D signal incorporating embedded features of the neighborhood characteristics, which can be used to extract different parameters in time-, frequency- and wavelet-domains. In the following, S was used as a general notation for signals correspond to any spatial location.

In time-domain three parameters were calculated. These parameters included the time-domain integrated backscattering (T_{IB}), time variance (T_{var}), and time entropy (T_E). The time-domain integrated backscatter (T_{IB}) parameter was evaluated as the average power of ultrasound backscattered signals and was described in decibel (dB) [26] as:

$$T_{IB}=20\log_{10}\left(\frac{\int_o^T S^2dt}{\int_o^T S_0^2dt}\right), \quad (2)$$

where S is the signal voltage within the kernel, S_0 the smallest voltage the system can detect, and T the integral interval. The second parameter was the time variance (T_{var}), which measures the dispersion of signal samples around their mean value evaluated as:

$$T_{var}=\frac{1}{(n+1)(m+1)-1}\sum_{x=1}^{(n+1)(m+1)}(S_x-M)^2, \quad (3)$$

where x is the sample number and M the mean value of S. In addition to these parameters, Shannon entropy was adopted as a statistical descriptor of ultrasound signal variability within a ROI in ultrasound imaging [27,28]. Shannon entropy (T_E) of S was calculated as:

$$T_E(S)=-\sum_x S_x^2\log\left(S_x^2\right), \quad (4)$$

where S is the envelop signal and S_x the coefficients of S in an orthonormal basis [29]. Note that T_{var} and T_E were evaluated using the envelop of ultrasound signals.

The second set of parameters was extracted from the frequency response of RF signals. Komiyama et al. [18] have performed several studies and reported the usefulness of using intravascular ultrasound integrated backscatter (F_{IB}) images to characterize atherosclerotic plaques in human arteries. Recently, our team reported that other parameters such as the variance (P_{var}) and maximum amplitude (P_{max}) of the power spectral density (PSD) of signal S can also be used for tissue characterization [23]. Here, similar procedures were

followed where Burg algorithm was used to estimate the PSD of signal S for each spatial location ($PSD_{i,j}$). Burg parametric method for PSD estimation overcomes the limited frequency resolution and spectral leakage effects of nonparametric estimation due to the finite length of data [30]. The PSD was estimated using Burg autoregressive (AR) prediction model for the signal S. In this work, the AR spectrum was calculated using a fast Fourier transform (FFT) of 1024 length, determined as next power of 2 from length of S (585). A 12th order AR model was adopted to avoid excessive smoothing in the PSD curve by using lower orders and hamming window was applied to minimize spectral leakage within the range of frequency (22–81 MHz). We evaluated F_{IB} as the normalized average power calculated using the integral of PSD over the transducer frequency bandwidth with respect to the PSD of a perfect reflector (PSD_{Ref}) [18], which is described as:

$$F_{IB}=10\log_{10}\left(\frac{\int PSD df}{\int PSD_{Ref} df}\right). \quad (5)$$

A glass plate of 2.4 mm thickness (⩾wavelength) perpendicular to ultrasound propagation was used as the perfect reflector.

The last set of parameters was calculated from the approximation coefficients of wavelet Daubechies 3 (db3). This kind of wavelet transformation is widely used in signal/image time–frequency analysis, subsampling and denoising due to its stability, and has been previously utilized in ultrasound applications [31]. In this work, single level discrete wavelet transform (DWT) was used to decompose original RF signals into half size approximation sequences without scarifying important frequency components within transducers' bandwidth. The wavelet approximation signal W was evaluated by applying MATLAB "dwt" function on the time signal S after normalization. Wavelet parameters such as the root mean square value (RMS) of the approximation signal (W_{rms}) and the integrated backscatter (W_{IB}) were used. Generally, RMS is a statistical measure of the magnitude of varying quantity. The RMS of the approximation signal (W_{rms}) was evaluated as:

$$W_{rms}=\sqrt{\frac{\sum_{n=1}^{N} w_n^2}{N}}, \quad (6)$$

where W_n is the wavelet approximation coefficient number n in W reconstructed from the ROI, and N the total number of coefficients in W. The parameter W_{IB} was evaluated using wavelet decomposition defined as:

$$W_{IB}=20\log_{10}\left(\frac{\int_o^K w^2 dk}{\int_o^K w_{Ref}^2 dk}\right). \quad (7)$$

where W_{Ref} is the wavelet coefficients of the reference echo. Since the first wavelet approximation was used in this study, K the integral interval length equals $T/2$.

Hybrid ultrasound images were reconstructed by calculating and assigning the value of each parameter in any domain to the center pixel(s) of the kernel. These procedures were repeated for all kernels within the ROI, suspected vessel lesion, selected for parametric analysis.

2.3. Tissue preparation and animal protocols

All animals were cared in accordance with the protocol approved by the Animal Care and Use Committee of the Health Science Center of West Virginia University. The generation and initial characterization of A_1 adenosine receptor knockout (A_1KO) mice on C57BL/6 background have previously been described by Schnermann et al. [32,33]. Previous study from this laboratory has shown a decrease in atherosclerosis development in DKO when compared to APOE-KO in the same age [5]. Ultrasound tissue characterization was tested to detect different progressions of atherosclerotic lesions in the DKO and APOE-KO mouse models. The C57BL/6 mouse has no atherosclerotic lesions and was used as control. Because atherosclerosis is known to be different between gender [34], all our mice compared between groups were of the same gender.

While mice were under deep anesthesia with pentobarbital sodium (100 mg/kg ip), a thoracotomy was performed. Aortas were gently extracted, and fat and connective tissue were carefully removed. Aorta was cut off at the base of the heart. *In vitro* experiments were conducted to investigate the efficacy of the system on reconstructing high-resolution B-mode and hybrid images for such small objects (diameter ≈ 1 mm). Studies were performed to image isolated aortas from different mouse types including the APOE-KO, DKO and control. Objects were placed approximately at the transducer focus on a layer of silicone gel lining a glass plate (perfect reflector) forming the reference echo as described earlier. RF signals were collected using a separation distance down to 8.5 μm between adjacent signals. Cross-sectional ultrasound scans down to 50 μm apart in the elevation direction were acquired for each mouse artery covering from the aortic sinus to the thoracic aorta. After ultrasound scanning, samples were sent to Research Histology Services at University of Pittsburgh for histology processing. Aortas were embedded in paraffin blocks, and then sectioned at 5 μm. Histology sections were stained using Masson Trichrome to highlight collagen as an indicator for fibrotic tissue. Fibrotic tissue was stained as blue, muscle filament was stained as red, and erythrocyte was stained as orange. In this study, short-axis ultrasound scans of the vessels were particularly acquired to match with the orientation of histology cross-sections during comparison. In order to correlate different plaque components with the values of ultrasonic parameters, ROIs were chosen within different cross-sections of the DKO and APOE-KO mouse models. The parameters' values were evaluated and compared with the pathologic characteristics using pathologic photographs and the ultrasound images such as in [26]. In this study, kernels within ROIs were set to one of three plaque components including calcification, fibrosis, and lipid pool.

Additionally, a pilot study was performed to test the *in vivo* feasibility of the tissue characterization technique using ultrasound data acquired via a commercially available ultrasound machine. Ultrasound B-mode images and raw data after beamforming were acquired using a high-frequency ultrasound machine for small animals imaging (Vevo 2100, VisualSonics Inc., Toronto, ON, Canada). Imaging procedures were performed using the MS 550D linear array transducer (22–55 MHz) of 40 MHz center frequency that can provide axial and lateral resolutions of 40 μm and 80 μm, respectively. Mice were anesthetized and maintained by isoflurane inhalation (1–3%) for up to 2 h. Supplemental heat and close monitoring of temperature, pulse and respiration were provided during study. The chest area was shaved and ultrasound gel was applied to maintain good coupling between the transducer and animal skin and minimize the air contents. Ultrasound transcutaneous scanning was performed for a 51-week female DKO and APOE-KO mice to acquire scans from the aortic arch and its branches, particularly at the area of the brachiocephalic artery. Lesions at the brachiocephalic artery, a small vessel (diameter ≈ 0.5 mm) connecting the aortic arch to the right subclavian and right carotid artery, are common sites for atherosclerosis development [35,36].

3. Results

B-mode ultrasound images for the short-axis views of isolated mouse aortas were reconstructed and compared with histology cross-sections to render approximately matched couples for further analyses. ROIs were manually segmented in B-mode images, and then quantitative hybrid images were reconstructed using the tissue characterization technique described earlier. Fig. 2 shows images for the aortic arches of 70-week control, 50-week DKO and APOE-KO mice. The adventitial layer was removed from all samples while keeping the intima and media layers, where the majority of atherosclerotic lesions are expected. Optical images acquired with the aid of microscope for the aortic arch of isolated aortas of the control, DKO, and APOE-KO mice are shown in Fig. 2a–c, respectively. The superimposed yellow dash lines indicate the location of the best-matched cross-sections used in both ultrasound imaging and histology analysis. Fig. 2d–f depicts B-mode images of selected cross-sections from control, DKO, and APOE-KO mice, respectively, while Fig. 2g–i shows the approximately-matched histology stained with Masson's trichrome. A morphological matching was observed between B-mode and histology sections.

Ultrasound hybrid imaging was preformed for selected cross-sections in Fig. 2 to characterize vascular tissue. Ultrasonic parameters in different domains were used to reconstruct six different images for the control, DKO, and APOE-KO mice in Fig. 3a–c, respectively. T_{IB} images in the first row were reconstructed using the time-domain integrated backscattering parameter that has been previously validated to characterize plaques in human arteries using intravascular ultrasound imaging (IVUS) [17]. T_{IB} images of the APOE-KO mouse (Fig. 3c) showed lesions of different levels of T_{IB} values at the aortic cross-section. Atherosclerotic plaques in APOE-KO mouse exhibited higher values of T_{IB} and larger lesions (Fig. 3c) than those observed in two cross-sections of control and DKO in Fig. 3a and b, respectively. The thick part of atheroma in the upper part (12 o'clock position) within the short-axis view (Fig. 3c) exhibited the highest dB value (highest contrast), however, other lesions diagnosed as atherosclerosis may show lower dB values such as the stenotic lesion in the middle. T_{IB} image of the DKO mouse (Fig. 3b) exhibited lesions of lower T_{IB} values (contrast) and distributed on areas smaller than of the APOE-KO mouse. On the other hand, T_{IB} image of the control mouse cross-section (Fig. 3a) exhibited, relatively, homogenous cross-section (low contrast) with some small lesions of medium scale dB values lower than those described in atherosclerotic mice (Fig. 3b and c). It was observed that the T_{IB} parameter showed the highest dB values, or highest contrast resolution, in hybrid images of the APOE-KO mice, followed by the DKO, and control mice, respectively, when using same dynamic ranges. Hybrid images for the same short-axis view were reconstructed (rows following T_{IB} in Fig. 3) using other parameters including time variance (T_{var}), time entropy (T_E), frequency integrated backscatter (F_{IB}), wavelet root mean square value (W_{rms}), and wavelet integrated backscatter (W_{IB}), respectively. For each parameter, images were reconstructed using the same dynamic range for fair comparisons. These ranges were selected to balance between the range of parameters' values and visualization contrast. Generally, hybrid images reconstructed using other ultrasonic parameters (second to sixth row in Fig. 3) exhibited noticeable contrast changes in vascular tissues in areas similar to those observed in the T_{IB} image when analyzing same cross-sections of the control, DKO, and APOE-KO mouse models as will be described (Fig. 4).

To quantify the assessment of atherosclerosis using hybrid imaging ultrasonic parameters, the mean value of each ultrasonic parameter was evaluated using n ROIs from the three mouse models near the bifurcation where atherosclerosis was expected. On the other hand, percentage (%) luminal occlusion, a parameter evaluated directly from histology was used to demonstrate the progression of atherosclerosis in the control, DKO, and APOE-KO mouse groups. Fig. 4a compared the mean and standard error ($p < 0.05$) of % luminal occlusion in

different mouse types evaluated using n histology segments near the bifurcation. As expected, the control group ($n = 5$) did not develop atherosclerosis and showed clear cross-sections. The APOE-KO group ($n = 5$) showed more progression of atherosclerosis of 75.71 ± 4.82% luminal occlusion, while the DKO group ($n = 4$) developed less luminal occlusion (51.81 ± 9.74%). Fig. 4b–g depicted the mean value of ultrasound parameters and the standard error ($p < 0.05$), which include T_{IB}, T_{var}, T_E, F_{IB}, W_{rms}, and W_{IB}, respectively. The bar plots compared the values of these parameters within the aortas of the control ($n = 6$), DKO ($n = 6$), and APOE-KO ($n = 10$) groups. The APOE-KO model showed segments of the highest ultrasonic parameters of −10.11 ± 1.92 dB, −12.13 ± 2.13 dB, −7.54 ± 1.45 dB, −5.10 ± 1.06 dB, −5.25 ± 0.94 dB, and −10.23 ± 2.12 dB in T_{IB}, T_{var}, T_E, F_{IB}, W_{rms}, and W_{IB} images, respectively. A significant decrease in the same ultrasonic parameters ($p < 0.05$) was observed in lesions within the DKO mouse as −17.84 ± 2.67 dB, −19.26 ± 4.92 dB, −13.48 ± 1.82 dB, −9.10 ± 1.29 dB, −9.15 ± 1.25 dB, and −18.28 ± 2.57 dB in hybrid images. The control mouse exhibited the lowest means of −20.20 ± 2.71 dB, −22.54 ± 4.54 dB, −14.94 ± 2.05 dB, −9.64 ± 1.34 dB, −10.20 ± 1.27 dB, and −19.36 ± 3.24 dB, using same parameters respectively.

Quantitative ultrasound parameters were measured at different ROIs that have been approximately matched with the histology of atherosclerotic lesions of DKO and APOE-KO mice, and were set to one of three plaque components including calcification, fibrosis, and lipid pool. Table 1 describes the mean and standard deviation of each ultrasound parameter evaluated for each plaque component. All parameters exhibited similar characteristics where calcified lesions (dark dense blue in histology images, $n = 6$) showed the highest values ($p < 0.05$) of −13.2 ± 9.4 dB, −16.3 ± 13.9 dB, −14.8 ± 8.8 dB, −10.1 ± 7.4 dB, −8.6 ± 5.2 dB, and −14.2 ± 9.4 dB using T_{IB}, T_{var}, T_E, F_{IB}, W_{rms}, and W_{IB}, respectively. Same parameters exhibited values of −32.5 ± 15.2 dB, −31.2 ± 10.1 dB, −26.7 ± 11.4 dB, −20.0 ± 8.3 dB, −18.5 ± 7.4 dB, and −31.3 ± 13.9 dB in fibrotic lesions (light blue in histology images, $n = 13$). Lesions of lipid pool (clear crystal in the histology images $n = 8$) exhibited values of −42.4 ± 3.5 dB, −45.0 ± 3.0 dB, −33.0 ± 4.7 dB, −21.5 ± 1.8 dB, −20.3 ± 2.2 dB, and −35.8 ± 5.2 dB using T_{IB}, T_{var}, T_E, F_{IB}, W_{rms}, and W_{IB}, respectively. Ultrasound hybrid imaging was used to estimate the area of calcified lesion within atherosclerotic plaque as a percentage (%) of vessel cross-sectional area within the aortic arch region for DKO and APOE-KO mice. Calcified lesions were determined using the threshold of the parameters' values depicted in Table 1 for calcification and areas were normalized to vessel cross-section. Fig. 5 compares % calcification evaluated from hybrid imaging using different parameters with those evaluated blindly using histology cross-sections. Calcified lesions were characterized in hybrid images of vessel cross-sections ($n = 4$) from the DKO and APOE-KO mice, while no signs of calcification were found in the control. Calcified lesion estimation errors of 0.02–3.6% can be observed in Fig. 5 by comparing histology and ultrasonic hybrid measurements.

In vivo B-mode images for a long-axis view for the aortic arch of 51-week old female DKO and APOE-KO mice are shown in the first row of Fig. 6. Yellow[1] rectangles are superimposed on B-scans to highlight ROIs at the brachiocephalic artery that was used in our analyses. Reference echoes were approximated as the strongest reflections within RF scans. *In vivo* ultrasound hybrid images were reconstructed for the ROI in each mouse type using T_{IB}, T_{var}, F_{IB}, and W_{IB} are shown in the following rows (second to fifth) in Fig. 6, respectively. Clean lumen was observed in Fig. 6a, where contrast changes in hybrid imaging within the vessel wall were observed. These findings could be a sign of mild atherosclerosis, if exists. However, luminal occlusions were observed in the APOE-KO

[1]For interpretation of color in Figs. 2 and 6, the reader is referred to the web version of this article.

vessel of Fig. 6b. Values of ultrasonic parameters in the range of dB measured for fibrosis and lipid pool (Table 1) were observed, which might indicate the existence of such plaque components. Additionally, higher ultrasonic parameters were observed within the vessel wall of APOE-KO mouse than those found in the DKO mouse (Fig. 6a). These *in vivo* results were in agreement with both *in vitro* and histology findings in assessing atherosclerosis within the DKO and APOE-KO mouse groups.

4. Discussion

This paper described an ultrasound-based imaging technique for diagnosing atherosclerosis and characterizing atherosclerotic plaque in small animals. The ability of hybrid set of images reconstructed using six ultrasonic parameters was tested to diagnose plaques in atherosclerotic mouse models. Ultrasonic parameters such as T_{IB} and F_{IB} [18,26] were used to reconstruct high-resolution (≤40 μm) images to characterize atherosclerotic lesions in mouse models. In addition, novel parameters such as T_{var}, T_E, W_{rms}, and W_{IB} were described and compared to T_{IB} and F_{IB} and histology. All parameters exhibited significant changes in their values ($p < 0.05$) in the hybrid imaging of control and atherosclerotic vascular tissues (Figs. 3 and 4). Atherosclerotic lesions in APOE-KO mice differed in ultrasonic parameters from control vascular ROIs by approximately 10 dB, 10.5 dB, 7.5 dB, 4.5, 5 dB, 9 dB in T_{IB}, T_{var}, T_E, F_{IB}, W_{rms}, and W_{IB} images (Figs. 3 and 4). Whereas, atherosclerotic lesions in DKO mice showed differences of approximately 2.5 dB, 2.0 dB, 1.5 dB, 1.0, 1.0 dB, 1.5 dB in T_{IB}, T_{var}, T_E, F_{IB}, W_{rms}, and W_{IB} images from control vascular ROIs, which are lower than those observed in APOE-KO lesions (Figs. 3 and 4). Ultrasound findings were in agreement with the matching histologically characterized vascular tissue from different mice (Figs. 2 and 3). Atherosclerotic vessels in the APOE-KO model (Fig. 3c) showed more progression of atherosclerosis than the DKO model (Fig. 3b) in hybrid imaging and higher values of all ultrasonic parameters (Fig. 4). However, both atherosclerotic models exhibited higher values of ultrasonic parameters than those measured in comparable vascular segments in the control mice (Figs. 3 and 4). In addition, the areas of atherosclerotic lesions in DKO mouse were smaller than those observed in the APOE-KO mouse (Figs. 3 and 6). This indicated slower atherosclerosis progression in the DKO mice and was in agreement with our previous finding [5]. We believe that the use of combined set of hybrid images for vascular tissue characterization instead of using a single parameter shall improve the diagnosis and monitoring of atherosclerosis and help developing automatic diagnostic technique.

A quantitative comparison between ultrasonic parameters (Fig. 4b–g) and histology (Fig. 4a) was performed at possible lesions where atherosclerosis is expected in the aortic arch region of the control, DKO, and APOE-DKO. Hybrid ultrasonic imaging exhibited the highest contrast between various lesions in the APOE-KO mice (Fig. 4b–g), with an emphasis that such technique could augment B-mode imaging to assess atherosclerotic plaques. On the other hand, these parameters showed lower dB values in the images of the control and the DKO mice than in the APOE-KO mice (Fig. 4b–g). These findings suggest a relationship between the value of ultrasonic parameters and atherosclerosis progression as shown in the bar plots in Fig. 4b–g. The change in ultrasonic parameters followed a similar trend to the percentage luminal occlusion evaluated from histology (Fig. 4a) in assessing the atherosclerosis progression in the three mouse models (control, DKO, and APOE-KO). However, lesions diagnosed with atherosclerosis might show different ranges of dB values based on the plaque components as explained in Table 1 for calcification, fibrosis, and lipid pool. In the comparison between plaque compositions from histopathology and hybrid imaging parameters (Table 1), it was found that calcified lesions exhibited the highest values for all parameters, followed by fibrosis, then lipid pool. These changes in ultrasonic parameters in different plaque compositions were in good agreement with those reported in

previous studies [17,37]. Kawasaki et al. [17] correlated the T_{IB} parameter with atherosclerotic components, where calcification exhibited the highest dB values, then mixed lesions of both calcification and fibrosis, followed by lesions of pure fibrosis, lipid pool, etc. In this study, only three plaque components were characterized including calcification, fibrosis, and lipid pool, since they showed significant differences in ultrasonic parameters ($p < 0.05$) as reported earlier [17,37]. The size of calcified lesions within atherosclerotic plaque, as a percentage of vessel cross-sectional area, was estimated using hybrid imaging, and then compared with histology estimation (Fig. 5). Using cross-sections from the aortic arch region of DKO and APOE-KO mice, estimation errors of 0.02–3.6% were reported in calculating % calcification between ultrasonic parameters and histology calculations. Parameters such as T_E and F_{IB} showed the lowest % calcification estimation error in both DKO and APOE-KO (Fig. 5).

In this paper, most studies were *in vitro* that require sacrificing the animal. In spite of showing the *in vivo* feasibility of the ultrasound hybrid imaging technique to characterize atherosclerotic plaques in DKO and APOE-KO mice (Fig. 6), further investigations are required. Investigations are needed to employ optimum procedures including reference echo standardization to overcome the transducer diffraction effect via employing dynamic focusing that increases the field of depth within the ROI, parameters' optimization, and validation using a large number of animals. Ongoing research in our laboratory focuses on applying such an *in vivo* technique, which will allow the long term monitoring of disease progression or treatment. This study showed the feasibility of diag nosing atherosclerosis and characterizing atherosclerotic plaque using only 2D hybrid imaging. In the future, this algorithm can be extended to include 3D hybrid imaging for the complete volume assessment of atherosclerosis progression.

Due to the small size of vascular cross-sections used in this study (≈1 mm), it was difficult to render exactly matched ultrasound and histology. However, we were able to render limited number of approximately matched vascular segments (n) in each mouse type to use throughout the analyses as presented in Figs. 4 and 5 and Table 1. A major limitation of this study is the relatively small number of animals that may not properly cover potential animal variations. However, the main goal of this study was to demonstrate the feasibility of using hybrid parameters to reliably characterize vascular tissue and validate histologically. Further statistical analysis and correlation studies are needed to assess the sensitivity of each ultrasonic parameter and correctly characterize atherosclerotic plaque and the specificity in identifying normal tissue. In this work, we used the first approximation of wavelet decomposition to calculate ultrasonic parameters (W_{rms} and W_{IB}) using Eqs. (6) and (7). The number of wavelet coefficients per kernel is half the number of time domain samples. Consequently, the number of computations was dropped by half size compared to other parameters calculated in the time domain. Further levels of decomposition may be tested, which could decrease the number of computations by factors of 4, 8, or less, and more parameters could be investigated as well.

5. Conclusion

An ultrasound-based hybrid imaging technique for vascular tissue diagnosis and plaque characterization in mice is described. This technique extracts six parameters from time-, frequency-, and wavelet-domains to reconstruct a set of ultrasound hybrid images. The technique was tested mainly using 55 MHz high-frequency ultrasound single-element imaging system providing maximum spatial resolution of 24 μm to characterize atherosclerotic plaques in three mouse models. Mouse models included the control C57BL/6, and atherosclerotic apolipoprotein E-knockout (APOE-KO) and APOE/A1 adenosine receptor double knockout (DKO) mice of different progression of atherosclerosis. Novel

parameters such as time variance (T_{var}), time entropy (T_E), wavelet RMS (W_{rms}), and wavelet integrated backscatter (W_{IB}), showed similar performance to the previously investigated parameters including time integrated backscatter (T_{IB}) and frequency integrated backscatter (F_{IB}), and histology findings in diagnosing atherosclerosis and characterizing the plaque. Atherosclerotic lesions in APOEKO mice exhibited differences in ultrasonic parameters from control vascular ROIs of approximately 10 dB, 10.5 dB, 7.5 dB, 4.5, 5 dB, 9 dB in T_{IB}, T_{var}, T_E, F_{IB}, W_{rms}, and W_{IB} images. Whereas, atherosclerotic lesions in DKO mice showed differences from control vascular ROIs of approximately 2.5 dB, 2.0 dB, 1.5 dB, 1.0, 1.0 dB, 1.5 dB in images, respectively, which were lower than those were observed in APOE-KO lesions ($p < 0.05$). Moreover, the *in vivo* feasibility of the hybrid technique was demonstrated using a 40 MHz linear array transducer attached to commercial ultrasound scanner for small animal imaging. Hybrid ultrasound images showed good agreement with histological finding and succeeded to quantitatively measure the percentage of calcified plaque tissue with maximum error of 3.5%. This technique can be implemented in any ultrasound machine providing RF accessibility. These findings demonstrated the potential use of ultrasound hybrid imaging for noninvasive vascular tissue diagnosis, which can be applied in both preclinical animal studies and human future clinical use. Ongoing research in our laboratory focuses on validating and testing the technique *in vivo* using larger sample size, and developing the 3D hybrid imaging for tissue characterization.

Acknowledgments

This work was supported by NIH-DE019561 to OMM, in part by NIH-HL027339 and HL094447 to SJM, Research Funding Development Grant of West Virginia University to BT, and NIH Instrumentation grant S10 RR026378 by KHM. Authors would like to thank Ms. Sarah McLaughlin for her help performing the ultrasound *in vivo* scanning and animal procedures.

References

[1]. U.S. Government. Chronic Disease Overview. 1999.

[2]. Rosamond W, Flegal K, Friday G, Furie K, Go A, Greenlund K, Haase N, Ho M, Howard V, Kissela B, Kittner S, Lloyd-Jones D, McDermott M, Meigs J, Moy C, Nichol G, O'Donnell CJ, Roger V, Rumsfeld J, Sorlie P, Steinberger J, Thom T, Wasserthiel-Smoller S, Hong YL, Assoc AH. Heart disease and stroke statistics – 2007 update – a report from the American Heart Association Statistics Committee and Stroke Statistics Subcommittee. Circulation. 2007; 115:E69–E171. [PubMed: 17194875]

[3]. Daugherty A. Mouse models of atherosclerosis. American Journal of the Medical Sciences. Jan. 2002 323:3–10. [PubMed: 11814139]

[4]. Meir KS, Leitersdorf E. Atherosclerosis in the apolipoprotein E-deficient mouse – a decade of progress. Arteriosclerosis Thrombosis and Vascular Biology. 2004; 24:1006–1014.

[5]. Teng B, Roush KP, Nadeem A, Morrison RR, Mustafa SJ. Reduced Atherosclerotic Lesions in A1 Adenosine Receptor (AR)/Apolipoprotein E (APOE) Double Knockout mice. Role for A1 AR in the Development of Atherosclerosis, July 1, 2009. Arteriosclerosis, Thrombosis, and Vascular Biology. 2009; 29:e73–74.

[6]. Baumgart D, Schmermund A, Goerge G, Haude M, Ge JB, Adamzik M, Sehnert C, Altmaier K, Groenemeyer D, Seibel R, Erbel R. Comparison of electron beam computed tomography with intracoronary ultrasound and coronary angiography for detection of coronary atherosclerosis. Journal of the American College of Cardiology. 1997; 30:57–64. [PubMed: 9207621]

[7]. Sakuma H, Kawada N, Takeda K, Higgins CB. MR measurement of coronary blood flow. Journal of Magnetic Resonance Imaging. 1999; 10:728–733. [PubMed: 10548782]

[8]. Chang GY, Cao F, Krishnan M, Huang M, Li ZJ, Xie XY, Sheikh AY, Hoyt G, Robbins RC, Hsial T, Schneider MD, Wu JC. Positron emission tomography imaging of conditional gene activation in the heart. Journal of Molecular and Cellular Cardiology. 2007; 43:18–26. [PubMed: 17467733]

[9]. Roper SN, Moores MD, Gelikonov GV, Feldchtein FI, Beach NM, King MA, Gelikonov VM, Sergeev AM, Reitze DH. In vivo detection of experimentally induced cortical dysgenesis in the adult rat neocortex using optical coherence tomography. Journal of Neuroscience Methods. 1998; 80:91–98. [PubMed: 9606054]

[10]. Aristizabal O, Christopher DA, Foster FS, Turnbull DH. 40-MHz echocardiography scanner for cardiovascular assessment of mouse embryos. Ultrasound in Medicine and Biology. 1998; 24:1407–1417. [PubMed: 10385963]

[11]. Sherar MD, Noss MB, Foster FS. Ultrasound backscatter microscopy images the internal structure of living tumor spheroids. Nature. 1987; 330:493–495. [PubMed: 3683563]

[12]. Sun L, Lien CL, Xu XC, Shung KK. In vivo cardiac imaging of adult zebrafish using high frequency ultrasound (45–75 MHz). Ultrasound in Medicine and Biology. 2008; 34:31–39. [PubMed: 17825980]

[13]. Sun L, Richard WD, Cannata JM, Feng CC, Johnson JA, Yen JT, Shung KK. A high-frame rate high-frequency ultrasonic system for cardiac imaging in mice. IEEE Transactions On Ultrasonics Ferroelectrics And Frequency Control. 2007; 54:1648–1655.

[14]. Thomas LJ, Wickline SA, Perez JE, Sobel BE, Miller JG. A real-time integrated backscatter measurement system for quantitative cardiac tissue characterization. IEEE Transactions on Ultrasonics Ferroelectrics and Frequency Control. 1986; 33:27–32.

[15]. Miller JG, Perez JE, Mottley JG, Madams EI, Johnhton PH, Blodgett ED, Thomas LJ III, Sobel BE. Myocardial tissue characterization: an approach based on quantitative backscatter and attenuation. 1983 IEEE Ultrasonics Symposium. 1983:782–793.

[16]. Bridal SL, Toussaint JF, Raynaud JS, Fornes P, Leroy-Willig A, Berger G. US backscatter and attenuation 30–50 MHz and MR T2 at 3 tesla for differentiation of atherosclerotic artery constituents in vitro. IEEE Transactions on Ultrasonics Ferroelectrics and Frequency Control. 1998; 45:1517–1525.

[17]. Kawasaki M, Takatsu H, Noda T, Sano K, Ito Y, Hayakawa K, Tsuchiya K, Arai M, Nishigaki K, Takemura G, Minatoguchi S, Fujiwara T, Fujiwara H. In vivo quantitative tissue characterization of human coronary arterial plaques by use of integrated backscatter intravascular ultrasound and comparison with angioscopic findings. Circulation. 2002; 105:2487–2492. [PubMed: 12034654]

[18]. Komiyama N, Berry GJ, Kolz ML, Oshima A, Metz JA, Preuss P, Brisken AF, Moore MP, Yock PG, Fitzgerald PJ. Tissue characterization of atherosclerotic plaques by intravascular ultrasound radiofrequency signal analysis: an in vitro study of human coronary arteries. American Heart Journal. Oct.2000 140:565–574. [PubMed: 11011329]

[19]. Nair A, Kuban BD, Obuchowski N, Vince DG. Assessing spectral algorithms to predict atherosclerotic plaque composition with normalized and raw intravascular ultrasound data. Ultrasound in Medicine and Biology. 2001; 27:1319–1331. [PubMed: 11731045]

[20]. de Korte CL, Hansen HHG, van der Steen AFW. Vascular ultrasound for atherosclerosis imaging. Interface Focus. 2011; 1:565–575. [PubMed: 22866231]

[21]. de Korte CL, Sierevogel MJ, Mastik F, Strijder C, Schaar JA, Velema E, Pasterkamp G, Serruys PW, van der Steen AFW. Identification of atherosclerotic plaque components with intravascular ultrasound elastography in vivo a Yucatan pig study. Circulation. 2002; 105:1627–1630. [PubMed: 11940537]

[22]. Mahmoud, AM.; Cortes, DH.; Mustafa, SJ.; Mukdadi, OM. High frequency precise ultrasound imaging system to assess mouse hearts and blood vessels. Proceedings of the ASME 2008 Summer Bioengineering Conference; FL. 2008.

[23]. Mahmoud, AM.; Teng, B.; Mustafa, SJ.; Mukdadi, OM. High-frequency tissue classification of atherosclerotic plaques in an APOE-KO mouse model using spectral analysis. Proceedings of the ASME International Mechanical Engineering Congress and Exposition (IMECE) 2009; FL. 2009. p. 505-508.

[24]. Frazier CH, O'Brien WD. Synthetic aperture techniques with a virtual source element. IEEE Transactions On Ultrasonics Ferroelectrics And Frequency Control. 1998; 45:196–207.

[25]. Li ML, Guan WJ, Li PC. Improved synthetic aperture focusing technique with applications in high-frequency ultrasound imaging. IEEE Transactions On Ultrasonics Ferroelectrics And Frequency Control. 2004; 51:63–70.

[26]. Kawasaki M, Takatsu H, Noda T, Ito Y, Kunishima A, Arai M, Nishigaki K, Takemura G, Morita N, Minatoguchi S, Fujiwara H. Noninvasive quantitative tissue characterization and two-dimensional color-coded map of human atherosclerotic lesions using ultrasound integrated backscatter – comparison between histology and integrated backscatter images. Journal of the American College of Cardiology. 2001; 38:486–492. [PubMed: 11499742]

[27]. Hughes MS, McCarthy JE, Marsh JN, Arbeit JM, Neumann RG, Fuhrhop RW, Wallace KD, Znidersic DR, Maurizi BN, Baldwin SL, Lanza GM, Wickline SA. Properties of an entropy-based signal receiver with an application to ultrasonic molecular imaging. Journal of the Acoustical Society of America. 2007; 121:3542–3557. [PubMed: 17552706]

[28]. Mahmoud, AM.; Mukdadi, OM.; Kadah, YM. Entropy based phase aberration correction technique in ultrasound imaging. Proceedings of the ASME Summer Bioengineering Conference; Keystone, Colorado, USA. 2007.

[29]. Coifman RR, Wickerhauser MV. Entropy-based algorithms for best basis selection. IEEE Transactions on Information Theory. 1992; 38:713–718.

[30]. Proakis, JG.; Manolakis, DG. Digital Signal Processing. Prentice-Hall; 2000.

[31]. Cincotti G, Loi G, Pappalardo M. Frequency decomposition and compounding of ultrasound medical images with wavelet packets. IEEE Transactions on Medical Imaging. 2001; 20:764–771. [PubMed: 11513027]

[32]. Sun, D.; Samuelson, LC.; Yang, T.; Huang, Y.; Paliege, A.; Saunders, T.; Briggs, J.; Schnermann, J. Mediation of tubuloglomerular feedback by adenosine: evidence from mice lacking adenosine 1 receptors. Proceedings of the National Academy of Sciences USA (PNAS); 2001. p. 9983-9988.

[33]. Teng B, Ansari HR, Oldenburg PJ, Schnermann J, Mustafa SJ. Isolation and characterization of coronary endothelial and smooth muscle cells from A1 adenosine receptor-knockout mice. American Journal of Physiology – Heart and Circulatory Physiology. 2006; 290:H1713–H1720. [PubMed: 16299260]

[34]. Thomas CM, Smart EJ. Gender as a regulator of atherosclerosis in murine models. Current Drug Targets. 2007; 8:1172–1180. [PubMed: 18045095]

[35]. Bentzon JF, Falk E. Atherosclerotic lesions in mouse and man: is it the same disease? Current Opinion in Lipidology. 2010; 21:434–440. [PubMed: 20683327]

[36]. Rosenfeld ME, Polinsky P, Virmani R, Kauser K, Rubanyi G, Schwartz SM. Advanced atherosclerotic lesions in the innominate artery of the ApoE knockout mouse. Arteriosclerosis Thrombosis and Vascular Biology. 2000; 20:2587–2592.

[37]. Okubo M, Kawasaki M, Ishihara Y, Takeyama U, Kubota T, Yamaki T, Ojio S, Nishigaki K, Takemura G, Saio M, Takami T, Minatoguchi S, Fujiwara H. Development of integrated backscatter intravascular ultrasound for tissue characterization of coronary plaques. Ultrasound in Medicine and Biology. 2008; 34:655–663. [PubMed: 18077081]

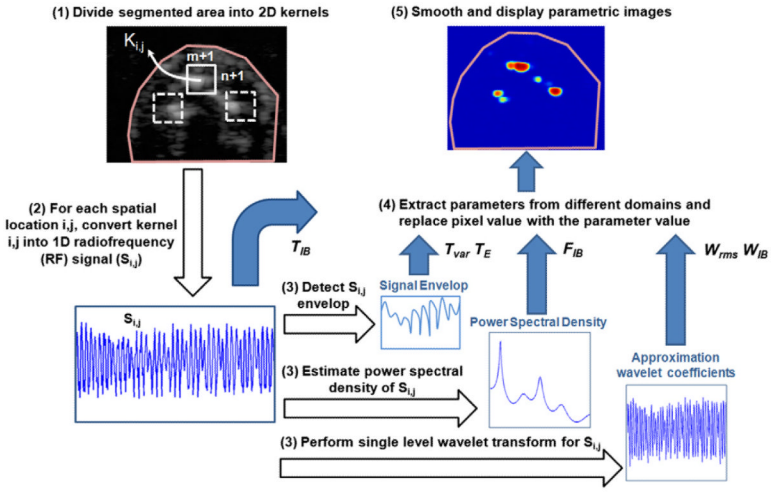

Fig. 1.

A schematic diagram describes the main steps of the hybrid ultrasound imaging algorithm. T_{IB}, T_{var}, T_E, F_{IB}, W_{rms}, and W_{IB} are time integrated backscatter, time variance, time entropy, frequency integrated backscatter, wavelet *RMS*, and wavelet integrated backscatter, respectively.

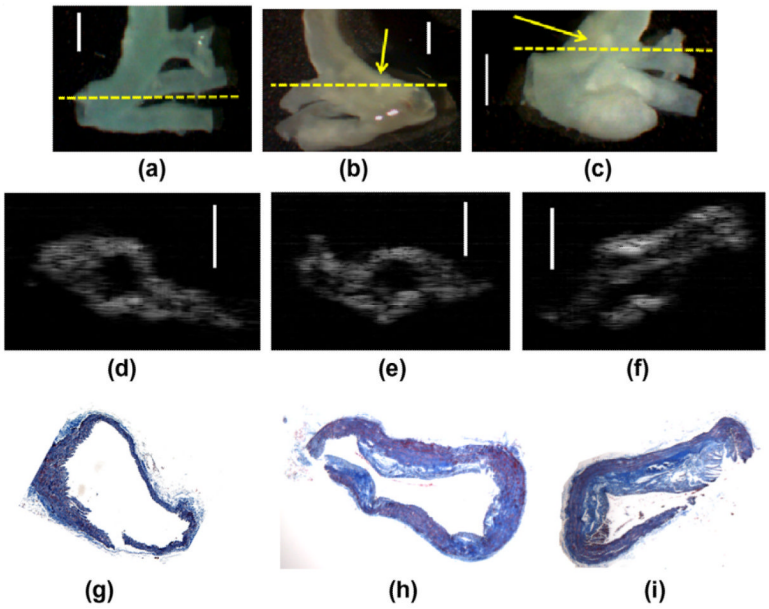

Fig. 2.

Different kinds of images for the aortic arch of control, DKO, and APOE-KO mice, respectively, after removing the adventitial layer. (a)–(c) Optical images acquired with the aid of microscope for the aortic arches of the control, DKO, and APOE-KO mice, respectively. Arrows highlight suspected atherosclerotic lesions. The dash lines indicate approximately cross-sections used in the following ultrasound imaging and histology, (d)–(f) ultrasound B-mode images for the cross-sections indicated by dash lines at the bifurcation of the control, DKO, and APOE-KO mice, respectively, and (g)–(i) approximately matched histology sections stained with Masson's trichrome for the cross-sections used in ultrasound imaging (d)–(f). Blue represents fibrotic tissue, red represents muscle filament, and orange represents erythrocytes (thrombus). Darker dense blue represents possible calcification area. Morphological matching is observed between various kinds of images (bar = 1 mm). (For interpretation of the references to color in this figure legend, the reader is referred to the web version of this article.)

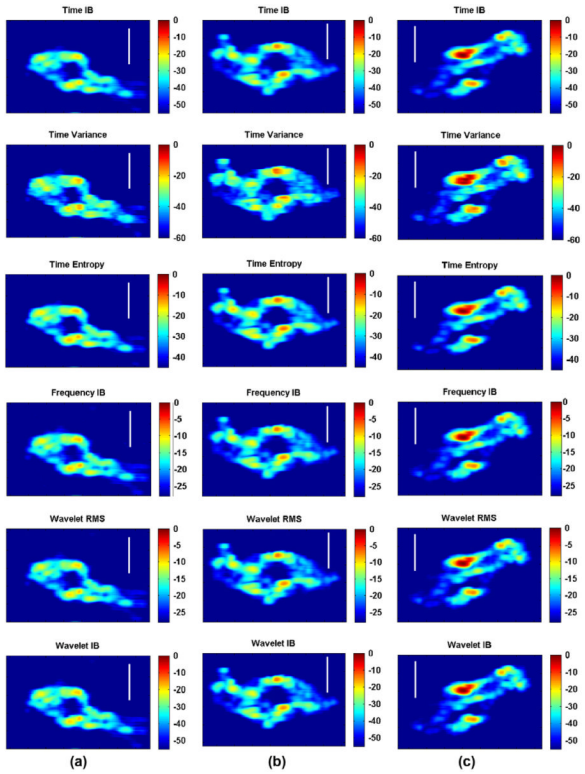

Fig. 3.

Ultrasound hybrid images for the cross-sections in Fig. 2 of the control, DKO, and APOE-KO mice. Images within the same row are reconstructed using same time, frequency, or wavelet parameter. From top to bottom, parameters include time integrated backscatter (T_{IB}), time variance (T_{var}), time entropy (T_E), frequency integrated backscatter (F_{IB}), wavelet RMS (W_{rms}), and wavelet integrated backscatter (W_{IB}), respectively. (a) Hybrid images of the control mouse, (b) DKO mouse, and (c) APOE-KO mouse. Generally, the APOE mouse (c) shows lesions of dB higher values (contrast) in all parameters distributed on larger areas than the DKO mice (b) and the control (a) (bar = 1 mm).

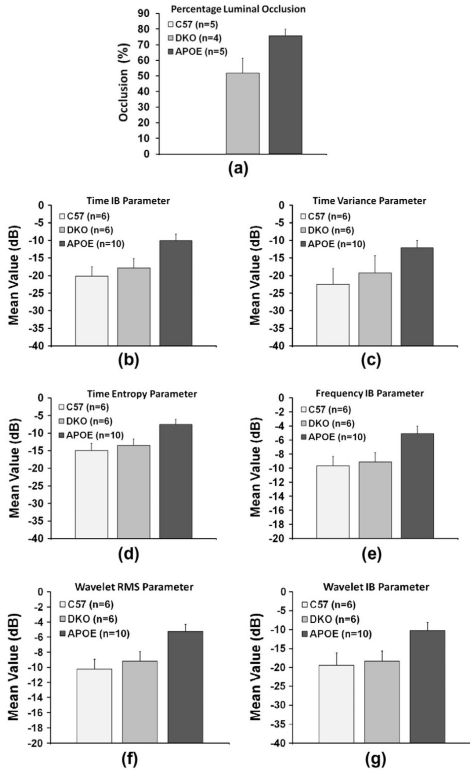

Fig. 4.

Bar plots compare findings of the histology and ultrasound hybrid imaging within the bifurcation of the aortic arch of different mouse models. (a) Percentage luminal occlusion, as an indication of atherosclerosis progression, in the control, DKO, and APOE-KO mouse models. (n = histology cross-sections), and (b)–(g) mean values of ultrasonic parameters including time integrated backscatter (T_{IB}), time variance (T_{var}), time entropy (T_E), frequency integrated backscatter (F_{IB}), wavelet RMS (W_{rms}), and wavelet integrated backscatter (W_{IB}) at corresponding lesions within of the control, DKO, and APOE-KO mouse models. (n = region of interests). Error bars represent the standard error ($p < 0.05$). The APOE-KO mouse showed the largest luminal occlusion followed by the DKO. Ultrasonic parameters showed similar behaviors to histology where all parameters showed the highest values for the APOE-KO mouse followed by the DKO.

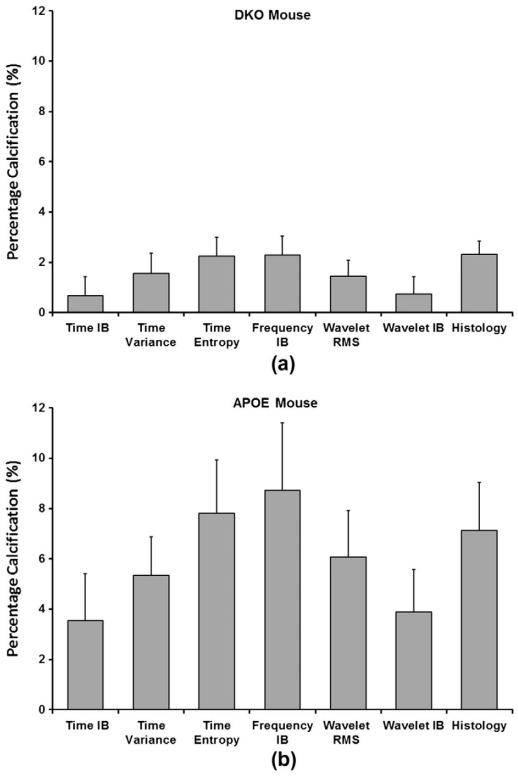

Fig. 5.

Measurements of calcified areas as a percentage of vessel cross-sections evaluated from ultrasound hybrid imaging and histology in atherosclerotic mice. (a) Percentage calcification calculated for a DKO mouse, and (b) percentage calcification calculated for an APOE-KO mouse. Ultrasound parameters include time integrated backscatter (T_{IB}), time variance (T_{var}), time entropy (T_E), frequency integrated backscatter (F_{IB}), wavelet RMS (W_{rms}), and wavelet integrated backscatter (W_{IB}), respectively. Cross-sections were acquired at the bifurcation of the aortic arch. Error bars represent the standard error ($p < 0.05$). Ultrasound parameters were able to detect calcified lesions and some parameters including T_E, F_{IB}, and W_{rms} showed good measurements agreement with histology for percentage calcification ($n =$ 4 cross-sections).

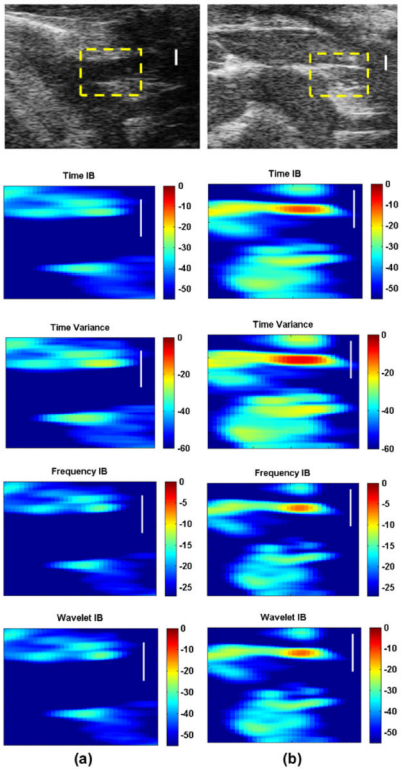

Fig. 6.

In vivo ultrasound images of long-axis views for the aortic arch area of 51-week-old (a) DKO mouse, and (b) APOE-KO mouse. Images, from top to bottom row, include B-mode with rectangles superimposed on the ROIs at the brachiocephalic artery, and ultrasound hybrid imaging of ROI using time integrated backscatter (T_{IB}), time variance (T_{var}), frequency integrated backscatter (F_{IB}), and wavelet integrated backscatter (W_{IB}), respectively. In the DKO mouse, clean vessel lumen is observed with small dB changes in parameters' values within the vessel wall. While at same location in the APOE-KO mouse a thickened vessel wall was observed with luminal occlusion and dB values higher than those observed in the DKO images in (a). These findings indicate more sever atherosclerotic plaque in the APOE-KO mouse (bar = 0.5 mm).

Table 1

The mean and standard deviation evaluated for each ultrasonic parameter at different components of atherosclerotic plaques including calcification, fibrosis, and lipid pool using n regions of interest matched with histology. Ultrasonic parameters include time integrated backscatter (T_{IB}), time variance (T_{var}), time entropy (T_E), frequency integrated backscatter (F_{IB}), wavelet RMS (W_{rms}), and wavelet integrated backscatter (W_{IB}).

Histology	Parameter mean ± 1 SD (dB)					
	T_{IB}	T_{var}	T_E	F_{IB}	W_{rms}	W_{IB}
Calcification (n = 6)	−13.2 ± 9.4	−16.3 ± 13.9	−14.8 ± 8.8	−10.1 ± 7.4	−8.6 ± 5.2	−14.2 ± 9.4
Fibrosis (n = 13)	−32.5 ± 15.2	−31.2 ± 10.1	−26.7 ± 11.4	−20.0 ± 8.3	−18.5 ± 7.4	−31.3 ± 13.9
Lipid pool (n = 8)	−42.4 ± 3.5	−45.0 ± 3.0	−33.0 ± 4.7	−21.5 ± 1.8	−20.3 ± 2.2	−35.8 ± 5.2